Progress In Electromagnetics Research C, Vol. 72, 55–63, 2017

Spiral Photon Sieves Apodized by a Bessel-Like Window

Jian Yu[1, 2], Shali Xiao[1], Tao Yi[2], Jin Li[2], Zhiwen Yang[2], and Shenye Liu[2, *]

Abstract—In order to improve the focusing and imaging effects of conventional spiral zone plates (SZPs), we design a new type of spiral photon sieve (SPSs) apodized by a robust Bessel-like window. The design principle and numerical simulation results show that the Bessel-like window has a better modulation effect on the main lobe compression and side suppression of the point spread function (PSF) than other traditional window. Taking advantage of the robustness of Bessel-like windows, the proposed SPS can achieve a higher spatial resolution and lower side lobe noise than the conventional SPS and SZP. The practical effects have also been demonstrated by image experiments on the micropore. Our work may find some potential applications in laser alignment, optical trapping, optical communication and edge enhancement imaging fields.

1. INTRODUCTION

A spiral zone plate (SZP) is an important type of diffractive optical element. It is often used in edge enhancement imaging, owing to its isotropic radial Hilbert transform function [1–3]. Due to the dark core structure of the focal spot, it also has a number of potential applications for astronomical observations and laser alignment [4–6]. In addition, the SZP has the potential for use in particle manipulation and optical communication, since it imparts an orbital angular momentum to the incident light [7, 8]. Unfortunately, as with a conventional Fresnel zone plate (FZP) [9], the spatial resolution of the SZP is limited by the width of its outermost zone. Moreover, the side lobe noise of the SZP increases significantly with increased topological charge number, similar to a spiral phase plate (SPP) [10, 11]. The inadequate spatial resolution and the serious side lobe noise hinder the use of an SZP in many cases, such as for edge enhancement imaging and multiple optical traps.

Due to the complexity of the design, there has been relatively little research into how to improve the characteristics of the SZP. To the best of our knowledge, only Bokor and Iketaki extended the conventional SZP to a Laguerre-Gaussian zone plate [2] and Xie et al. extended the conventional SZP to an SPS apodized by a digital prolate spheroidal window [12]. Compared to a conventional SZP, to some extent, the Laguerre-Gaussian zone plate reduces the side lobe noise, but its spatial resolution is still limited by the width of its outermost zone. Both the spatial resolution and the side lobe noise of the SPS are better than that of the conventional SZP due to the advantages of the design and modulation of traditional photon sieves (PS) [13]; however, with the digital prolate spheroidal window, the main lobe compression and side lobe suppression effects of the point spread function (PSF) are still not optimal because the suppression of the side lobes takes place with non-ignorable main lobe expansion.

In fact, due to its small size, light weight and flexible design, the photon sieve has seen great development since it was invented [13–16]. So far, a large number of diffractive optical elements based on this type of multi-micropore structure have emerged, such as flat helical nanosieves [17] and ultrahigh-capacity non-periodic photon sieves [18]. The amplitude, phase and polarization of the diffracted light

Received 15 November 2016, Accepted 14 February 2017, Scheduled 1 March 2017

* Corresponding author: Shenye Liu (yjyouxiang2015@sina.com).

[1] College of Optoelectronic Engineering, Chongqing University, Chongqing 400044, China. [2] Research Center of Laser Fusion, China Academy of Engineering Physics, P. O. Box 919-986, Mianyang 621900, China.

field behind these multi-micropore structures can be effectively controlled by adjusting the geometry positions and sizes of individual holes with an excellent transmittance modulation window function or other algorithm. In this paper, we extend a conventional SZP to an SPS apodized by a Bessel-like modulation window in visible light to optimize the spatial resolution and suppress the side lobe noise. Then the reasons that the proposed SPSs have optimal focusing and imaging effects will be discussed in detail. The improvement in spatial resolution and the side lobe noise will also be shown in the following sections.

2. DESIGN AND ANALYSIS

In fact, the Bessel-like window was proposed to completely suppress the side lobe noise of the SPP in [19]. According to Chen et al., the side lobes arise from diffraction by the margins as well as the center section of the SPP. Although the manufacture of the SPP with the Bessel-like modulation is very difficult, the modulation effect of a Bessel-like window is ideal since it takes advantage of the special integral formula of the Bessel function and the optimal modulation parameters. If we use the same Bessel-like window to modulate the transmission of the SZP/SPS, the Fresnel diffraction pattern at the focal plane will be given by the following integral formula in polar coordinates

$$\begin{aligned} E_p(\rho,\varphi) &= \frac{1}{i\lambda f}\int_0^R\int_0^{2\pi}\left[f_p(r)\,SZP_p(r,\theta)\right]\exp\left(i\frac{\pi r^2}{\lambda f}\right)\times\exp\left[\frac{2\pi\rho r}{\lambda f}\cos(\theta-\varphi)\right]rdrd\theta \\ &= (-i)^{p+1}\frac{k}{f}\exp(ip\varphi)\int_0^R J_{p+1}(\alpha r)J_p\left(\frac{k}{f}\rho r\right)dr \end{aligned} \tag{1}$$

where p is the topological charge number, λ the wavelength, f the focus length, k the wave number, (r, θ) the polar coordinates in SZP/SPS plane, (ρ, φ) the polar coordinates in the focal plane, $SZP_p(r, \theta)$ the phase function of the SZP [1], and $f_p(r)$ the Bessel-like window function. Equation (1) ignores the quadratic phase factor. $f_p(r)$ is used in the following expression to better suppress the side lobes of the optical vortex with a small topological charge [19, 20].

$$f_p(r) = \frac{J_{p+1}(\alpha r)}{r} \tag{2}$$

where $\alpha = \gamma_{p+1,1}/R$, $\gamma_{p+1,1}$ is the first root of the $(p+1)$ order Bessel function of the first kind, and R is the maximum radius of the SZP/SPS. Equation (1), above, is very similar to Equation (3) in [19], which means that the same modulation approach can be applied to improve the SZP/SPS and that the side lobes of the SZP/SPS also arise from diffraction at the center and margins. In order to overcome the spatial resolution limitation by the width of the outermost zone and suppress the side lobe noise, to take advantage of the design flexibility, in this paper we propose an SPS apodized by the Bessel-like window.

The following will introduce the specific design method of the SPS apodized by the Bessel-like window. The boundary of the SZP is defined by the following curve equations [5]

$$p\theta = (n+1/2)\pi + \frac{kr^2}{2f} \tag{3}$$

where $n = 0, \pm1, \pm2, \pm3 \ldots$. In keeping with the design method of a traditional PS, we replace the clear zones of the SZP by a large number of nonoverlapping pinholes to create an SPS. We also define a zone to be the rotation area when the clear helical structure is rotated 2π radian from the inside to the outside. The design parameters of the SPS are as follows: $\lambda = 532\,\text{nm}$, $f = 100\,\text{mm}$, $d/w = 1.5$, $\delta = 4.7\,\mu\text{m}$, where d is the pinhole diameter, w the width of the local zone of the underlying SZP, and δ the minimum feature size. Fig. 1(a) clearly shows the design process of a single ring in the SPS with a topological charge number $p = 1$. The binarized double-spiral plane structure represents a conventional SZP with $p = 1$, where the white zones are transparent, and the black zones are opaque. The red circles represent the transparent pinholes used to replace the clear zone in the conventional SZP. The transmission of the SPS can easily meet the criteria of a Bessel-like window function by

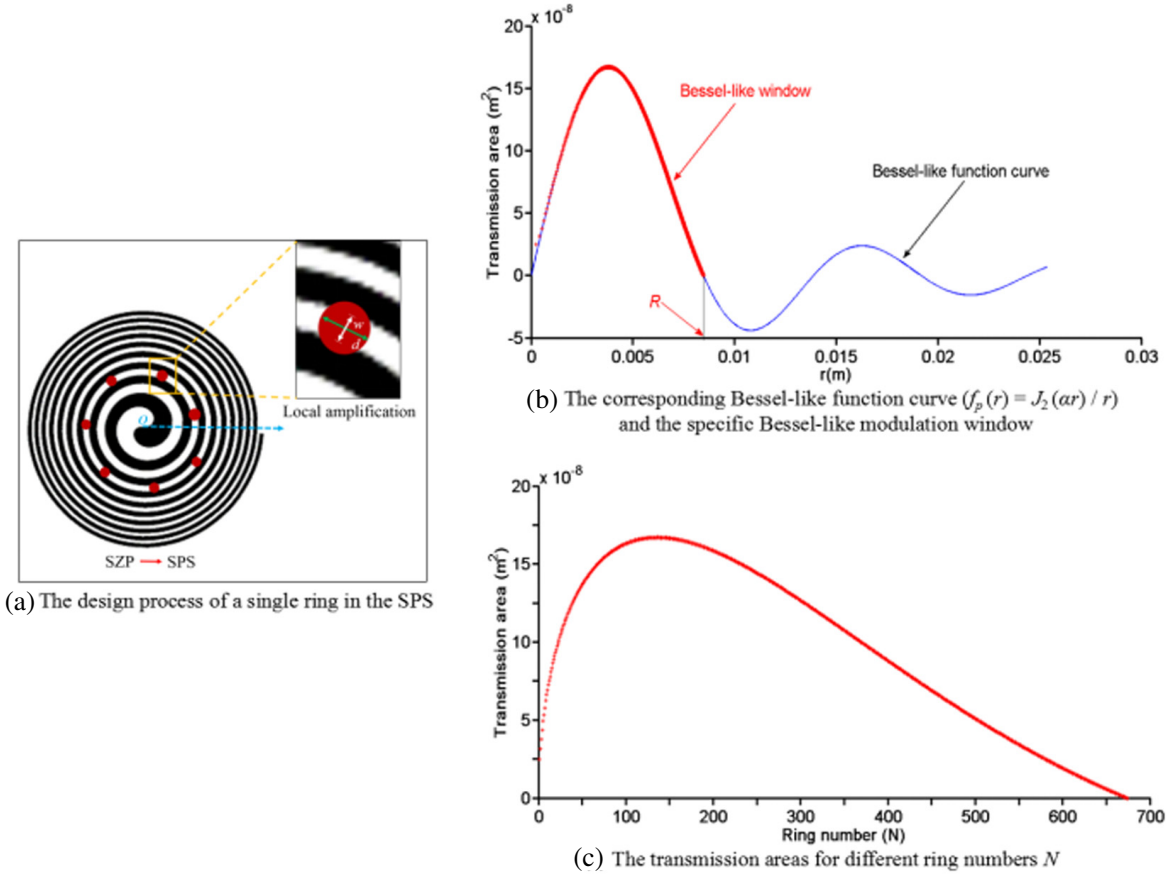

(a) The design process of a single ring in the SPS

(b) The corresponding Bessel-like function curve ($f_p(r) = J_2(\alpha r)/r$) and the specific Bessel-like modulation window

(c) The transmission areas for different ring numbers N

Figure 1. Design process of the SPS with topological charge number $p = 1$.

flexibly adjusting the positions of the pinholes for each zone. In addition, due to a simple binarized plane structure, the fabrication is not difficult. Fig. 1(b) shows the corresponding Bessel-like function curve ($f_p(r) = J_2(\alpha r)/r$) and the specific Bessel-like modulation window. When $r = R$, the modulation range of the Bessel-like window along the radial direction will be cut off. We also show the transmission areas of different ring numbers N in Fig. 1(c).

An SPS with different topological charges can realize edge enhancement imaging of an object with different spiral phase contrasts, so we have designed the SPS with an arbitrary topological charge. However, given the practicalities of the existing processing technology, we only test the SPSs with a small p, here. Schematic views of the SPS with topological charge numbers $p = 1$, 2, 3, 4 are shown in Fig. 2.

According to the Fresnel diffraction integral formula and the superposition principle for a light field, any point field distribution on the focal plane of an SPS is the summation of the contributions of all the pinholes, when using a plane wave as the incident illumination. The focal spot images of the SZP and SPS shown in Fig. 3 demonstrate that destructive interference occurs in the center of all focus spots and that the spot size increases as p increases. If the topological charge and minimum feature size stay constant, the numerical aperture (NA) of the SPS is larger than that of the SZP. Hence, the SPS has a substantially better spatial resolution, according to the Rayleigh resolution criterion. With the Bessel-like window's modification, due to the low side lobe noise, the vortex spots of SPS are simpler and cleaner.

Figure 4 shows the normalized PSF of the SZP ($p = 1$) and SPS ($p = 1$) apodized by several different windows. Some important parameters for each case are given in the figure, where ΔR_{core}, ΔR_{ring} and SM represents the FWHM of the dark core diameter, the FWHM of the doughnut-shaped ring width, and the ratio of the secondary to the principal maximum, respectively. When the SZP/SPS is considered

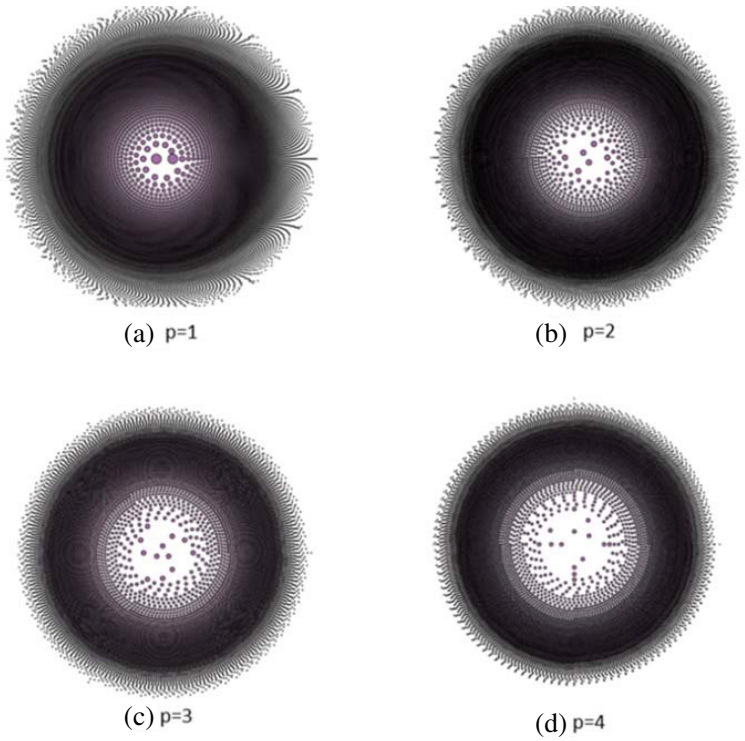

Figure 2. Schematic views of the SPS with different topological charge.

as a focusing and imaging element, ΔR_{core} determines the magnification, since a larger ΔR_{core} means that any two point sources on the object appear farther apart. By combining the topological charge number with the object-image distance, we can change the magnification easily. Here, unlike for a conventional FZP, the PSF of the SZP/SPS shows a double-peaked structure, so ΔR_{ring} is considered to be the spatial resolution of the SZP/SPS [21]. Reducing ΔR_{ring} will improve the spatial resolution of the apparatus. In addition, since the influences arising from the secondary maximum have serious repercussions for the signal-to-noise ratio of the focusing and imaging image, the parameter *SM* should also be as low as possible.

According to the curves and data in Fig. 4, the Bessel-like window has better effects in main lobe compression and side lobe suppression than the conventional SZP and SPS apodized by the conventional Blackman or Hanning windows. ΔR_{ring} of the SPS apodized by a Bessel-like window is 3.1 μm. ΔR_{ring} of the three other cases are 4.0, 3.3, 3.4 μm, respectively. Most notably, the SM of the SPS apodized by a Bessel-like window can be as low as 0.36%. However, the SM of the SZP and SPS apodized by the Blackman and Hanning windows are as high as 1.92%, 3.87%, 2.13%. There are two reasons that the SPS apodized by a Bessel-like window has advantages over the other types: (1) a Bessel-like window with optimal modulation parameters can effectively suppress the side lobes arising from the diffraction of the center and marginal sections of the SPS, since it can appropriately modulate transmission through those areas; (2) the suppression of the side lobes takes place with negligible main lobe expansion [19, 20]. The Blackman and Hanning windows, on the other hand, only appropriately modulate transmission at the marginal part, similar to a Laguerre-Gaussian window or a digital prolate spheroidal window. Thus, they are not able to effectively suppress the side lobes arising from the diffraction of the center. Additionally, main lobe expansion is non-negligible when using Blackman or Hanning windows. Also note that only the Bessel-like window has a lower SM than the SZP. The transmission curve of the SZP shows that the center and marginal transmission of the SZP is inherently low [22]. Thus, the proportion of the transmission through center is higher using the Blackman or Hanning window than for the conventional SZP. As a result, an SPS apodized by a Blackman or Hanning window has a higher SM than the conventional SZP. However, the inherent transmission of the SZP is not optimal for side lobe suppression compared with the modulation effects of the robust Bessel-like window.

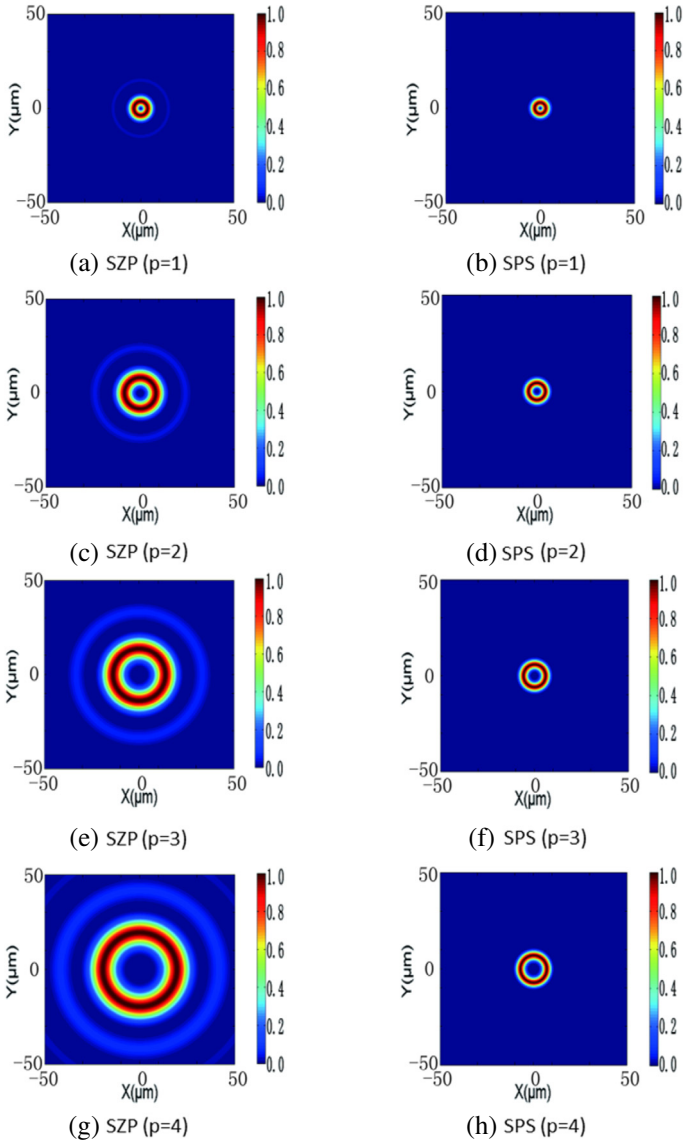

Figure 3. Focal spot profiles of the conventional SZP and the SPS apodized by the Bessel-like window.

Figures 5 and 6 show the normalized PSF of the SZP and the SPS apodized by the Bessel-like window for p values from 0 to 5. It is worth noting that the SZP with $p = 0$ corresponds to the conventional FZP, and the SPS with $p = 0$ corresponds to the conventional PS. When $p = 0$, there is no helical phase to give the incident illumination, so the SZP/SPS does not have a radial Hilbert transform function [1]. This means that the SZP/SPS ($p = 0$) cannot realize edge enhancement imaging. Also, since the PSF of an SZP/SPS ($p = 0$) is single-peaked rather than double-peaked ($\Delta R_{\text{core}} = 0$), ΔR_{ring}, which represents the FWHM of the single-peak, is considered to be the spatial resolution. As the charge number of the SZP increases from 0 to 5, ΔR_{core} of the PSF are 0, 3.5, 10.5, 19.3, 28.9, and 39.8 μm; ΔR_{ring} are 4.9, 4.0, 6.3, 8.2, 10.1, and 11.7 μm; the SM are 1.75%, 1.92%, 3.62%, 5.38%, 7.15%, and 8.78%, respectively. For the PSF of the SPS, ΔR_{core} are 0, 2.8, 5.6, 8.2, 10.6, and 12.9 μm; ΔR_{ring} are 4.1, 3.1, 3.3, 3.5, 3.6, and 3.6 μm; the SM are 0.09%, 0.36%, 0.59%, 0.77%, 0.95%,and 1.13%, respectively. Comparing ΔR_{ring} of the SZP under different p, only SZP ($p = 1$) has a better spatial resolution than that of SZP ($p = 0$). However, for the SPS, $p = 1$, 2, 3, 4, 5, all have a better spatial resolution than the SPS ($p = 0$). It can be predicted that, for the SPS, the spatial resolution will be lower than that for the SPS ($p = 0$) if p continues to increase. For $p = 0$, the SPS has a better spatial

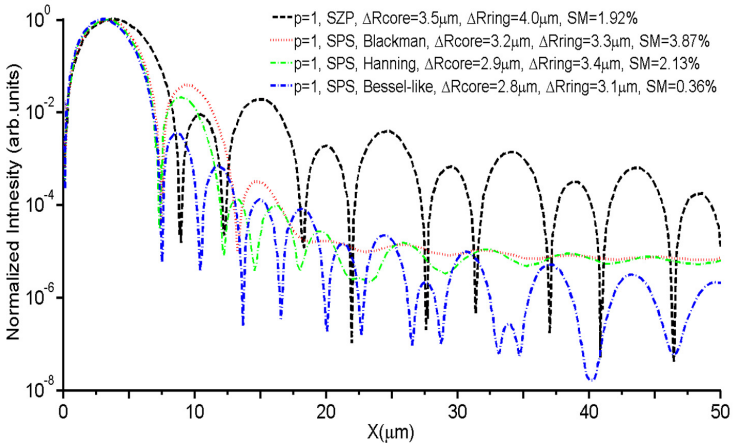

Figure 4. PSF of the conventional SZP and the SPS apodized by different windows.

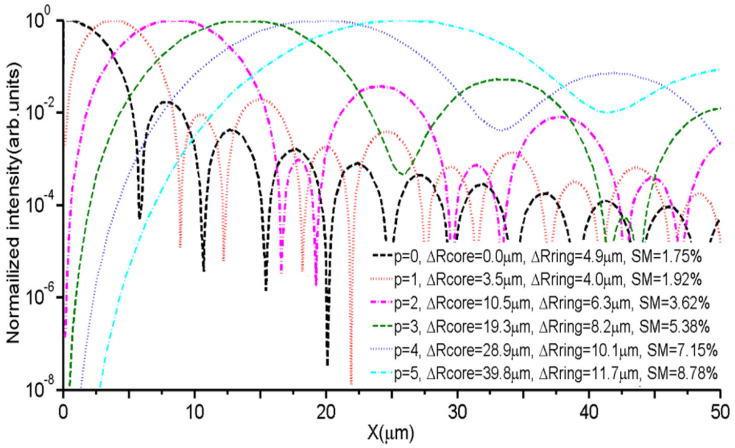

Figure 5. PSF of the conventional SZP.

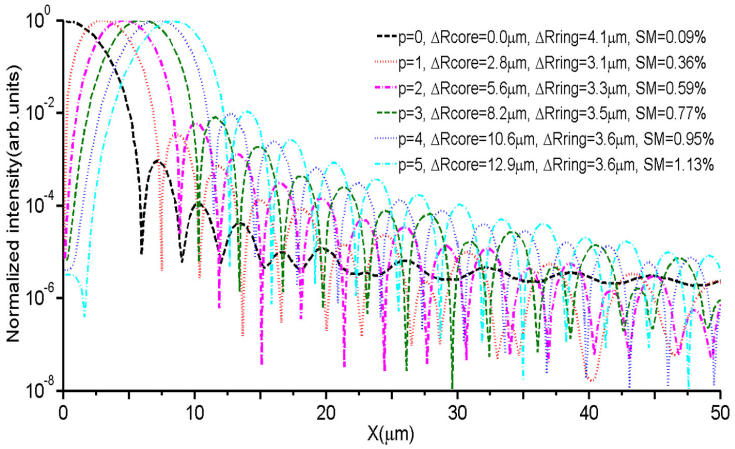

Figure 6. PSF of the SPS apodized by the Bessel-like window.

resolution than the SZP, and, more importantly, the intensity of the side lobes of the SPS is extremely low. If $p \neq 0$, because the selected clear zones are not radially symmetric, the difference between the transmission values for the actual modulation and the real Bessel-like window will increase slowly as p increases. This also leads to a very slow increase in the SM values. Depending on the robustness of Bessel-like window, however, all SM of the SPS are still very low. To sum up, for p values from 0 to 5, the reduced dark core diameters are 0, 0.7, 4.9, 11.1, 18.3, and 26.9 μm; the improved spatial resolutions are 0.8, 0.9, 3.0, 4.7, 6.5, and 8.1 μm; the improved SM are 1.66%, 1.56%, 3.03%, 4.61%, 6.20%, and 7.65%, respectively.

3. EXPERIMENTAL SIMULATION

A conventional SZP can achieve isotropic edge enhancement imaging for the amplitude object or phase object in a single step by combining the radial Hilbert transform filtering function with the FZP focusing function. The design of the SPS apodized by the Bessel-like window is based on the conventional SZP, so it also has the same isotropic edge enhancement imaging effect. In order to compare the imaging effects of the SZP and SPS, we take the micropore with a diameter 30 μm as an example and carry out a numerical simulation of its imaging experiments. In the simulation, we choose the first-order SZP and first-order SPS in turn as imaging devices. The magnifications of the images are set to 1.

Figure 7(a) shows the micropore picture, where the white area is clear, and the black area is opaque. Figs. 7(b) and (c) show the isotropic edge enhancement imaging results of the micropore by using the SZP and SPS, respectively. However, the imaging effects have an obvious difference in Fig. 7(b) and Fig. 7(c). In Fig. 7(b), there is a large amount of noise around the ring structure, which is usually called the "relief effect". This effect is mainly caused by the side lobes of the PSF of SZP, and its presence often leads to wrong interpretations, especially in the field of medical imaging. As we can see in Fig. 7(c), the ring image is very clear, and there is almost no interference noise. In fact, this effect results from the efficient side lobe suppression of the Bessel-like window. In addition, comparing the two imaging results carefully, we also see that the ring widths of the ring images are quite different. Figs. 7(e) and (f) show the normalized intensity distribution curves from the center of the ring image to

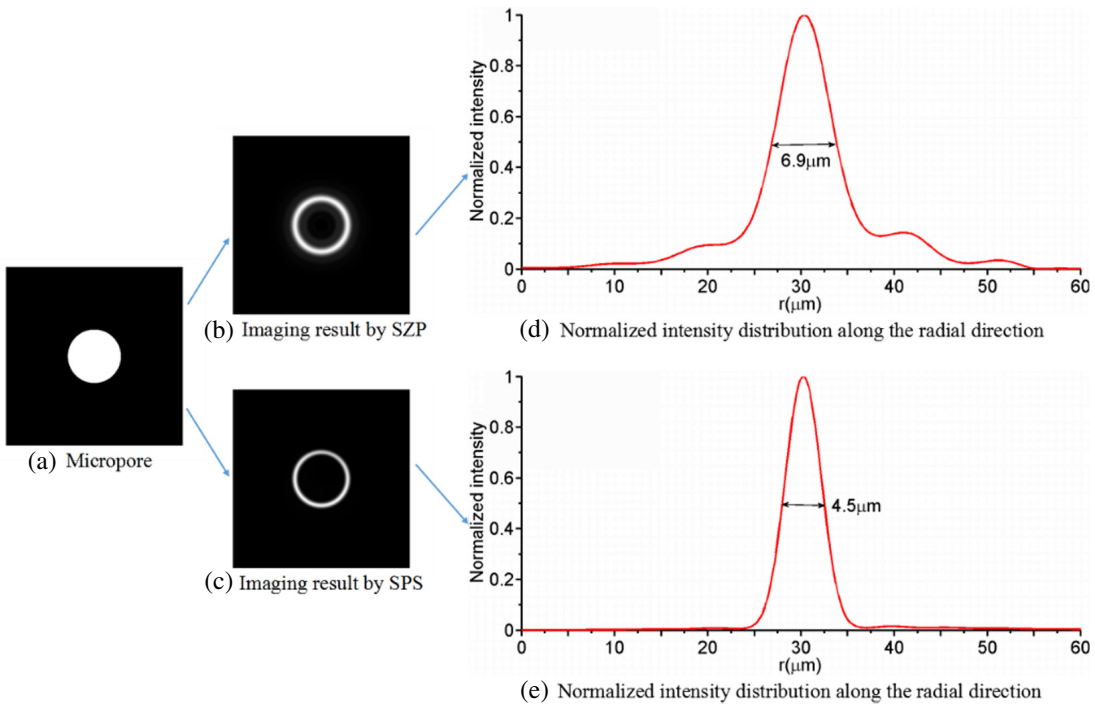

Figure 7. Numerical simulation results of the micropore imaging.

the edge of the ring image, respectively. According to the normalized intensity distribution data along the radial direction, we see that the FWHM of the ring in Fig. 7(e) is 6.9 μm, and the FWHM of the ring in Fig. 7(f) is 4.5 μm.

4. CONCLUSION

In conclusion, taking advantage of the robustness of Bessel-like windows, the SPS has a higher spatial resolution and lower side lobe noise than a conventional SPS and SZP. In edge enhancement imaging, the image quality will be improved greatly. Of course, due to these improvements, the SPS is also very useful for the astronomical observations, laser alignment and particle trap fields. Finally, it is also worth noting here that the diffraction efficiency of the SPS is lower than that of the SZP since pinholes have replaced the original clear zones. Fortunately, this disadvantage can be remedied by using high intensity sources, such as third-generation synchrotron light sources, since this allows the SPS to be used close to its diffraction efficiency limit.

ACKNOWLEDGMENT

The authors acknowledge support from the Beijing Institute of Microelectronics, Chinese Academy of Sciences. Our work is supported by the National Natural Science Foundation of China (Grant Nos. 11405158).

REFERENCES

1. Sakdinawat, A. and Y. W. Liu, "Soft-x-ray microscopy using spiral zone plates," *Opt. Lett.*, Vol. 32, 2635–2637, 2007.
2. Bokor, N. and Y. Iketaki, "Laguerre-Gaussian radial Hilbert transform for edge-enhancement Fourier transform x-ray microscopy," *Opt. Express*, Vol. 17, 5533–5539, 2009.
3. Sharma, M. K., R. K. Singh, J. Joseph, and P. Senthilkumaran, "Fourier spectrum analysis of spiral zone plates," *Opt. Commun.*, Vol.304, 43–48, 2013.
4. Mawet, D. E. Serabyn, J. K. Wallace, and L. Pueyo, "Improved high-contrast imaging with on-axis telescopes using a multistage vortex coronagraph," *Opt. Lett.*, Vol. 36, 1506–1508, 2011.
5. Heckenberg, N., R. McDuff, C. Smith, and A. White, "Generation of optical phase singularities by computer-generated holograms," *Opt. Lett.*, Vol. 17, 221–223, 1992.
6. Luo, D., C. Kuang, X. Hao, and X. Liu, "High-precision laser alignment technique based on spiral phase plate," *Opt. Laser. Eng.*, Vol. 50, 944–949, 2012.
7. Ng, J., Z. Lin, and C. T. Chan, "Theory of optical trapping by an optical vortex beam," *Phys. Rev. Lett.*, Vol. 104, 103601, 2010.
8. Gibson, G., J. Courtial, M. Padgett, M. Vasnetsov, V. Pas'ko, S. M. Barnett, and S. Franke-Arnold, "Free-space information transfer using light beams carrying orbital angular momentum," *Opt. Express*, Vol. 12, 5448–5456, 2004.
9. Chao, W., J. Kim, S. Rekawa, P. Fischer, and E. H. Anderson, "Demonstration of 12 nm resolution Fresnel zone plate lens based soft x-ray microscopy," *Opt. Express*, Vol. 17, 17669–17677, 2009.
10. Lin, J., X. C. Yuan, S. H. Tao, and R. E. Burge, "Variable radius focused optical vortex with suppressed sidelobes," *Opt. Lett.*, Vol. 31, 1600–1602, 2006.
11. Guo, C. S., Y. J. Han, J. B. Xu, and J. P. Ding, "Radial Hilbert transform with Laguerre-Gaussian spatial filters," *Opt. Lett.*, Vol. 31, 1394–1396, 2006.
12. Xie, C. Q., X. L. Zhu, L. Shi, and M. Liu, "Spiral photon sieves apodized by digital prolate spheroidal window for the generation of hard-x-ray vortex," *Opt. Lett.*, Vol. 35, 1765–1767, 2010.
13. Kipp, L., M. Skibowski, R. Johnson, R. Berndt, R. Adelung, S. Harm, and R. Seemann, "Sharper images by focusing soft X-rays with photon sieves," *Nature*, Vol. 414, 184–188, 2001.
14. Cheng, G., C. Hu, P. Xu, and T. Xing, "Zernike apodized photon sieves for high-resolution phase-contrast x-ray microscopy," *Opt. Lett.*, Vol. 35, 3610–3612, 2010.

15. Andersen, G., "Membrane photon sieve telescopes," *Appl. Opt.*, Vol. 49, 6391–6394, 2010.
16. Zhao, X., J. Hu, F. Xu, A. Zhu, and C. Wang, "Wide field-of-view imaging with wavefront coded diffractive photon sieves," *IEEE Photonics J.*, Vol. 8, 1–8, 2016.
17. Mei, S., M. Q. Mehmood, S. Hussain, K. Huang, X. Ling, S. Y. Siew, H. Liu, J. Teng, A. Danner, and Qiu, C., "Flat helical nanosieves," *Adv. Funct. Mater.*, Vol. 26, 1–8, 2016.
18. Huang, K., H. Liu, F. J. Garcia-Vidal, M. Hong, B. Luk'yanchuk, J. Teng, and C. W. Qiu, "Ultrahigh-capacity non-periodic photon sieves operating in visible light," *Nat. commun.*, Vol. 6, 1–7, 2015.
19. Chen, J., X.-C. Yuan, X. Zhao, Z. Fang, and S. Zhu, "Generalized approach to modifying optical vortices with suppressed sidelobes using Bessel-like functions," *Opt. Lett.*, Vol. 34, 3289–3291, 2009.
20. Chen, J., X. Zhao, Z. Fang, S. Zhu, and X.-C. Yuan, "Explicit relations and optimal parameters for sidelobe suppression in optical vortices with a modified Bessel function," *J. Opt. Soc. Am. A*, Vol. 27, 935–940, 2010.
21. Palacios, D., "An optical vortex coherence filter," Ph.D. Thesis, 2004.
22. Yi, T., L.-F. Cao, G.-H. Yang, S.-S. Liu, X.-L. Zhu, C.-Q. Xie, and J.-J. Dong, "Edge enhancement imaging using spiral zone plate," *High Power Laser and Particle Beams*, Vol. 22, 2075–2078, 2010.